Journal of Thermal Biology 74 (2018) 281–289

Contents lists available at ScienceDirect

Journal of Thermal Biology

journal homepage: www.elsevier.com/locate/jtherbio

Effect of tumor properties on energy absorption, temperature mapping, and thermal dose in 13.56-MHz radiofrequency hyperthermia

Bibin Prasad[a], Subin Kim[b], Woong Cho[b], Suzy Kim[b], Jung Kyung Kim[c,*]

[a] Department of Mechanical Engineering, Graduate School, Kookmin University, Seoul 02707, Republic of Korea
[b] Department of Radiation Oncology, SMG-Seoul National University Boramae Medical Center, Seoul 07061, Republic of Korea
[c] School of Mechanical Engineering and Department of Integrative Biomedical Science and Engineering, Graduate School, Kookmin University, 77 Jeongneung-ro, Seongbuk-gu, Seoul 02707, Republic of Korea

ARTICLE INFO

Keywords:
Hyperthermia
Tumor property
Energy absorption
Temperature mapping
Mouse model
Thermal dose

ABSTRACT

Computational techniques can enhance personalized hyperthermia-treatment planning by calculating tissue energy absorption and temperature distribution. This study determined the effect of tumor properties on energy absorption, temperature mapping, and thermal dose distribution in mild radiofrequency hyperthermia using a mouse xenograft model. We used a capacitive-heating radiofrequency hyperthermia system with an operating frequency of 13.56 MHz for in vivo mouse experiments and performed simulations on a computed tomography mouse model. Additionally, we measured the dielectric properties of the tumors and considered temperature dependence for thermal properties, metabolic heat generation, and perfusion. Our results showed that dielectric property variations were more dominant than thermal properties and other parameters, and that the measured dielectric properties provided improved temperature-mapping results relative to the property values taken from previous study. Furthermore, consideration of temperature dependency in the bio heat-transfer model allowed elucidation of precise thermal-dose calculations. These results suggested that this method might contribute to effective thermoradiotherapy planning in clinics.

1. Introduction

Mild hyperthermia (39–44 °C) is a complimentary therapeutic technique used in conjunction with radiation and chemotherapy to enhance therapeutic effectiveness (van der Zee, 2002). To integrate the use of hyperthermia therapy in clinics, hyperthermia-treatment planning tools are used to optimize cancer-treatment quality with the help of computational simulations. Generation of a computational model, calculation of power deposition, and determination of temperature distribution and thermal dosing are the major steps in hyperthermia-treatment planning (Paulides et al., 2013). Additionally, the dielectric properties of tissues should be carefully identified to allow accurate energy and thermal dose calculations. Several studies reported the dielectric properties of normal tissues over a wide range of frequencies (Gabriel et al., 1996a, 1996b, 1996c); however, additional studies are needed to understand the behavior of tumor properties, especially at frequency ranges < 50 MHz.

In hyperthermia-treatment planning using electromagnetic fields, dielectric property values are vital for the calculation of specific absorption rates (SAR) and thermal doses. The energy absorption of biological tissues in electromagnetic fields depends upon their relative permittivity (dielectric constant) and electrical conductivity with respect to a specific frequency (Joines et al., 1994). With increases in frequency, the relative permittivity and conductivity are expected to change by maintaining the same trend from low to high frequencies (Gabriel et al., 1996a, 1996b, 1996c). For frequencies < 100 MHz, increases in the dielectric properties of tumor tissues results from the charging of cell membranes, with minor contributions from protein constituents and ionic diffusion along the tissue surface (Foster and Schepps, 1981). For frequencies > 100 MHz, the dielectric properties of tissues can be explained based on the percentage of water content in the tissues, with tumors speculated to have higher water content than the surrounding normal tissues (Foster and Schepps, 1981; Joines et al., 1994). In general, tumors exhibit relatively high electrical conductivity and relative permittivity as compared with normal tissues; however, previous studies reported that some tumors exhibit similar or lower conductivity and permittivity values as compared with normal tissues (Joines et al., 1994; Yoo, 2004).

Unlike normal tissues, conductivity and permittivity values in tumors differ and are subject to change according to the organ or tissues in which they grow (Yoo, 2004). A previous study reported that for frequencies ranging from 50 MHz to 100 GHz, the permittivity and

* Corresponding author.
E-mail address: jkkim@kookmin.ac.kr (J.K. Kim).

https://doi.org/10.1016/j.jtherbio.2018.04.007
Received 12 January 2018; Received in revised form 20 April 2018; Accepted 20 April 2018
Available online 23 April 2018

conductivity of malignant tissues in organs, such as bladder, colon, liver, lymph nodes, mammary glands, spleen, and testis, were higher than that in normal tissues; however, few tumors, such as those in the kidney and lung, showed lower permittivity than the normal tissues, and the lung tumor showed lower conductivity relative to the normal tissues (Joines et al., 1994). Few studies have measured the dielectric properties of tumors using mouse models (Raoof et al., 2013; Rogers et al., 1983; Yoo, 2004). One group measured properties associated with brain, gastric, breast, and colon tumors from 500 MHz to 5 GHz, reporting that all tumors exhibited relatively high dielectric properties as compared with normal tissues; however, each of those tumor-specific dielectric properties was similar (Yoo, 2004). A study of normal tissues, liver, and pancreatic tumors reported that tumors exhibited higher dielectric properties than normal liver and pancreas tissue. Additionally, they reported that the values for the liver tumors were higher than those of pancreatic tumors within a frequency range of 10 MHz to 3 GHz (Raoof et al., 2013). Moreover, liver-tumor measurements from 100 MHz to 5 GHz in four cancer patients showed that tumors in each patient displayed a different dielectric property, with one patient having relatively low permittivity values relative to normal liver tissues due to pathological changes (Peyman et al., 2015). Variations in dielectric properties were also reported in colorectal cancer tissues at different tumor stages across a frequency range of 50–500 MHz (Li et al., 2017).

In addition to frequency specific dielectric properties, temperature dependence associated with thermal properties, metabolic heat generation, and perfusion should also be considered while determining temperature distribution and thermal dose. Most previous studies did not consider variations in properties for simulations of mild and ablative hyperthermia-temperature ranges (Kok et al., 2017, 2014; Oh et al., 2014; Zastrow et al., 2010; Zorbas and Samaras, 2014). A previous study showed that optimal dielectric and thermal-property values can partially neglect the effect of perfusion in hyperthermia-treatment planning (Ahmed et al., 2008). Other studies on temperature dependence in biological tissues showed that thermal properties are dependent on temperature (Bhattacharya and Mahajan, 2003; Choi et al., 2013). Additionally, consideration of variations in metabolic heat generation and blood perfusion is a better predictor of accurate heat transfer in tissues than using normothermic values associated with these properties (Rai and Rai, 1999). Therefore, accurate calculation of the thermal dose for numerical simulations requires determination of the effects of thermal properties, perfusion, and metabolic heat generation. Few hyperthermia studies with tissue mimicking phantoms showed good temperature mapping in experiments and simulations using measured dielectric properties of normal and tumor phantoms (Kim and Lee, 2015; Oh et al., 2014).

Previously, we reported temperature measurements using a phantom model and patient-specific simulations in real human-anatomy models to demonstrate selective heating characteristics and electrode optimization of treatment planning (Hossain et al., 2016; Prasad et al., 2016). In the present study, the effect of tumor properties on calculating energy absorbance and thermal dose was determined based on dielectric property measurement and temperature-dependent thermal properties, perfusion, and metabolic heat generation.

2. Materials and methods

2.1. Measurement of dielectric properties

The dielectric property measurement involves the measurement of complex permittivity, which consists of relative permittivity and imaginary permittivity and can be defined as follows:

$$\varepsilon^*(\omega) = \varepsilon'(\omega) - j\varepsilon''(\omega) \quad (1)$$

where $\varepsilon^*(\omega)$ is the complex permittivity, ω is the angular frequency, $\varepsilon'(\omega)$ is the relative permittivity or dielectric constant, $\varepsilon''(\omega)$ is the imaginary permittivity or dielectric loss factor. Imaginary permittivity can be converted into effective conductivity as follows:

$$\sigma = \omega\varepsilon_0\varepsilon'' \quad (2)$$

where σ is the conductivity, and ε_0 is the permittivity of free space.

According to a previously reported procedure (Raoof et al., 2013), fresh tumor samples (2 cm) excised sharply from mice were used for the measurements, which were performed using an Agilent 85070E high-temperature coaxial dielectric probe connected to an Agilent E4991A impedance analyzer, with a manufacturer uncertainty of 5% (Agilent Technologies, Santa Clara, CA, USA) (Raoof et al., 2013) across the frequency range 10–1000 MHz. Repeated measurements were performed for accuracy, and theoretical fitting of the measurement was accomplished using the dielectric dispersive-fitting tool available in Sim4Life software (https://www.zurichmedtech.com/sim4life/), with an accurate fitting achieved using a multi-pole Lorentz model (Banks et al., 2008; Stoykov et al., 2003; Sullivan, 1992).

$$\varepsilon^*(\omega) = \varepsilon_\infty + \sum_{p=1}^{P} \frac{a_p \Delta\varepsilon \omega_p^2}{\omega_p^2 + 2j\omega\delta_p - \omega^2} + \frac{\sigma}{j\omega\varepsilon_0} \quad (3)$$

where ε_∞ is the infinity permittivity, $\Delta\varepsilon$ is the difference between static and infinity permittivity, ω_p is the angular frequency of pole, a_p is the amplitude of pole, δ_p is the damping frequency of pole and, σ is the electric conductivity.

2.2. In vivo mouse experiments

Experiments were performed on a human tumor xenograft model. The local ethical committee for animal experiments approved the experimental protocol used in this study (17–0110-S1A1). Cancer cells (squamous cell carcinoma of the lung) were injected into the femoral region and allowed to grow until reaching 200 mm^3. A radiofrequency (RF) capacitive-heating device (LAB EHY 100; Oncotherm, Budapest, Hungary) with an operating frequency of 13.56 MHz was used for the experiments (Kim et al., 2018). Fiber optic temperature sensors were inserted into the tumor and surrounding tissues to estimate temperature increases and output power during RF heating. The experimental scheme involving the RF generator, electrode, data-acquisition temperature measurement, and sedating system is shown in Fig. 1(a). Initially, the mouse was kept in a chamber with circulating isoflurane gas for sedation, followed by transfer to a position above the heating system. To keep the mouse sedated throughout the experiment, isoflurane gas mixed with oxygen was administered through an inhaler. Four fiber optic sensors were placed 1) inside the tumor (5 mm from the electrode), 2) in nearby tissue (2 mm from the tumor), 3) in the rectum, and 4) toward the middle of the mouse at the interface between mouse and bed [Fig. 1(b)]. The positions of the sensors were chosen at the center region of the tumor to ensure heat transfers through the tumor, at the closest possible surrounding tissue to attain the temperature of tissue near the tumor, in the rectum to obtain variations in core body temperature, and at the interface between bed and skin to maintain body heat during experiment. Measurements were recorded using a data-acquisition system connected to a computer. The response time of the sensors was 9 s for sensor 1, 20 s for sensor 2, 67 s for sensor 3, and 81 s for sensor 4. Electrodes used for RF heating were placed on the tumor region and subjected to water cooling [Fig. 1(c)]. A total of four tumor-induced mice were used for the experiments, with each mouse treated four times over a 2-week period. The tumor was heated to 42 °C and maintained at that temperature for 30 min to establish a heating protocol.

2.3. Numerical simulation

Numerical simulations comprised a combination of electromagnetic and thermal simulations. All simulations were performed using the

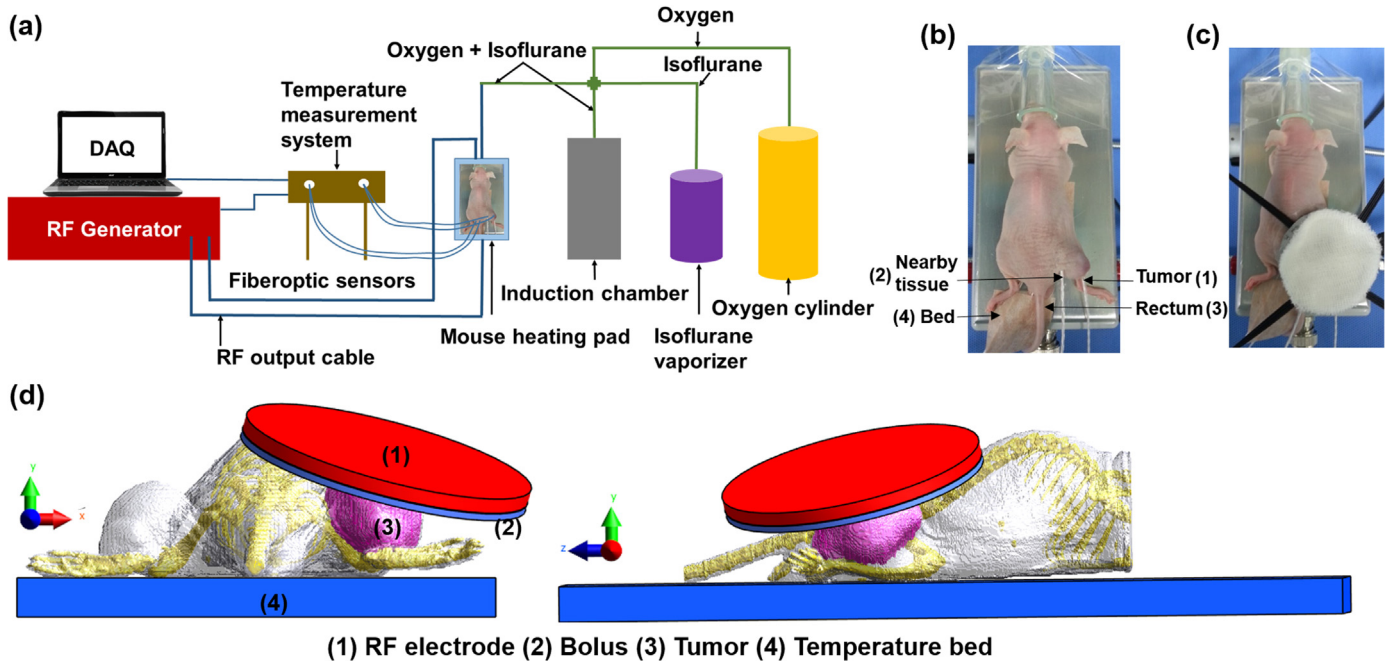

Fig. 1. (a) Experimental scheme for in vivo mouse experiments. (b) Sensor and electrode positions in tumor and nearby tissues. (c) Computational 3D mouse model used for simulations.

multiphysics simulation software Sim4Life (Kok et al., 2017; Prasad et al., 2016; Tomura et al., 2017). The quasi-static approximation in Maxwell's equation was used to calculate the potential distributions and energy distributions (Kok et al., 2017; Kok and Crezee, 2017; Tsuda et al., 1996) for capacitive RF heating. The governing equations are given as follows:

$$\nabla(-\varepsilon\nabla\varphi) = 0, \quad E = -\nabla\varphi \tag{4}$$

$$SAR = \frac{\sigma}{2\rho}|E|^2 \tag{5}$$

$$Q_r = \rho SAR = \frac{\sigma}{2}|E|^2 \tag{6}$$

where $\nabla\varphi$ is the electric potential, E is the electric field strength, SAR is the specific absorption rate, ρ is the mass density, and Q_r is the heat source.

The RF energy absorbed from electromagnetic simulation was provided as a user-defined heat source to the Pennes bioheat-transfer model to determine the thermal distribution (Pennes, 1948):

$$\rho c\frac{\partial T}{\partial t} = \nabla\cdot(k\nabla T) - \rho_b c_b\omega_b(T - T_b) + Q_r + Q_m \tag{7}$$

For temperature dependence, bioheat-transfer model was modified as follows:

$$\begin{aligned}\rho(c_a\Delta T + c_{ref})\frac{\partial T}{\partial t} &= \nabla\cdot((k_a\Delta T + k_{ref})\nabla T)\\ &\quad - \rho_b c_b(\omega_{b,a}\Delta T + \omega_{b,ref})(T - T_b) + Q_r\\ &\quad + (Q_{m,a}\Delta T + Q_{m,ref})\end{aligned} \tag{8}$$

where c is the specific heat, T is the temperature, t is the time, k is the thermal conductivity, Q_m is the metabolic heat-generation rate, ω_b is the perfusion rate, and ρ_b, c_b, and T_b correspond to the density, specific heat, and temperature of blood, respectively. c_a, k_a, $\omega_{b,a}$, $Q_{m,a}$, c_{ref}, k_{ref}, $\omega_{b,ref}$, and $Q_{m,ref}$ are the temperature-dependent coefficients and normothermic values associated with specific heat, thermal conductivity, perfusion and metabolic heat generation.

The amount of heat absorbed by tissues during thermal treatment can be quantified as the thermal dose, which is represented as cumulative equivalent minutes (CEM; at 43 °C) (Sapareto and Dewey, 1984). This provides the time–temperature relationship in equivalent minutes and can be expressed as follows:

$$CEM_{43} = \int_{t_0}^{t_{final}} R^{43-T(t)}dt \tag{9}$$

where R is the temperature dependence of the rate of cell death, with $R = 0.5$ for $T > 43$ °C, $R = 0.25$ for 39 °C $\leq T \leq$ 43 °C, and $R = 0.00$ for $T < 39$ °C. Additionally, dt is the time interval, T is the average temperature during time interval dt, and t_o and t_{final} are the initial and final heating periods, respectively.

Fig. 1(d) shows the three-dimensional (3D) computational domain using a mouse model and RF-electrode heating system. The mouse model was reconstructed from computed tomography images of mice used for experiments. An output power ranging from 1.5 W to 2.5 W was provided by the electrode, and an operating frequency of 13.56 MHz was used. A convective boundary with an ambient temperature of 25 °C and a surface heat-transfer coefficient of 5 W/m^2 K were used as boundary conditions. An initial temperature of 25 °C was used for the water bolus, and 27.7 °C was used for all body sites considered, with a simulation time of 45 min. Dielectric and thermal properties used in the simulation are listed in Table 1. All properties other than those of the tumors were obtained from the Sim4Life database (IT'IS Foundation, Zurich, Switzerland) (Hasgall et al., 2015). Measured dielectric properties were used for the tumor, and other properties were taken from the literature (Kok et al., 2014; Raoof et al., 2013). Cubic voxels with 1.98 M cells were used for the computation, with a time-step factor of 1. Grid-independent studies were conducted from coarser to finer meshes for accuracy.

3. Results and discussion

Dielectric property measurement trends across the frequency ranges correlated with previously reported measurements (Hasgall et al., 2015; Raoof et al., 2013; Rogers et al., 1983; Yoo, 2004). Fig. 2(a,b) shows the relative permittivity and calculated conductivity from imaginary permittivity across the frequency range 10–1000 MHz. The values of tumor properties were higher as compared with those of the surrounding tissue (Raoof et al., 2013) across the entire frequency range, mainly due

Table 1
Dielectric (13.56 MHz) and thermal properties of materials used in simulations.

Material	Relative permittivity	Electric conductivity (S/m)	Density (kg/m^3)	Specific heat (J/kg·K)	Thermal conductivity (W/m·K)	Heat generation (W/kg)	Perfusion (mL/min/kg)
Skin	285.24	0.238	1109	3390.5	0.3721	1.64	106.38
Bone	30.57	0.045	1908	1312.8	0.32	0.15	10
Rectum	217.11	0.512	1088	3657.5	0.542	11.85	786.23
Mouse tumor	278.85[a]	0.7847[a]	1070	3421.2	0.4949	0.9	18.36
Mouse tumor (previous study)	266.99	0.683	1070	3421.2	0.4949	0.9	18.36
Distilled water	76.7	0.00005	1000	4181.3	0.563	–	–

[a] measured dielectric properties.

to the dipolar reorientation of protein dipoles and charging of cell membranes (Foster and Schepps, 1981). The measured properties of muscular tumors at 13.56 MHz (Table 1) were used for the simulation. To ensure measurement accuracy, the permittivity and conductivity values were fitted with a three-pole Lorentz model, with the measurements fitting well with the theoretical model [Fig. 2(a,b)].

To standardize a heating protocol for our studies, multiple in vivo temperature measurements were performed on mice. Fig. 3 shows the power and temperature measurements taken during RF exposure and the calculated energy estimation. As shown in Fig. 3(a,b), within a short period of time and in a power range of 1.5–2.5 W, tumor temperature could be raised to 42 °C and maintained at that temperature for 30 min. We observed that the temperature of the surrounding normal tissues was much lower than that of the tumor tissues. When the final temperature in the tumor reached 42.2 °C, the nearby tissue, body, and bed temperatures were 35.03 °C, 30.98 °C, and 28.88 °C, respectively, revealing selective heating characteristics. Fig. 3(c, d) shows the energy, temperature, and time relationships for selective tumor heating based on the experimental measurements. Using an electrical energy of ~1500 J, the tumor could be selectively heated up to 42 °C, and at ~3500 J, the temperature in the tumor could be maintained at 42 °C for 30 min [Fig. 3(c)]. To interpret the relationship between energy, temperature, and time, correlations were predicted to determine the energy required to reach and maintain 42 °C with respect to time [Fig. 3(d)].

Simulations were performed to determine the energy absorption and temperature distribution inside the mouse anatomy. The absorbed energy and distributed temperature in the mouse-tumor volume are shown in Fig. 4(a,b). Fig. 4(a) shows the SAR distribution along the cross-section of the tumor and surrounding regions in the XY and YZ planes. A high degree of energy was absorbed in the tumor because of its high electrical conductivity and permittivity relative to the normal tissue. Additionally, we observed deposition of a mass-averaged SAR of 120.2 W/kg in the tumor region, followed by 7.18 W/kg toward the skin and further lower levels in other regions of the body. These results indicated an apparent difference in energy deposition during RF-induced heating between the tumor and surrounding normal tissue. As shown in cross-sectional planes XY and YZ [Fig. 4(b)], due to the high energy absorption, high temperature increases were observed in the tumor region, whereas the temperatures in surrounding normal tissues were much lower, thereby suggesting selective tumor heating [Fig. 4(c)].

Temperature measurements were mapped along with those of the simulations, revealing agreement between the results [Fig. 5(a)]. A comparison made by mapping the temperature increase in the mouse tumor with measured dielectric properties and property values from a previous study (Raoof et al., 2013) (Table 1) revealed notable differences in the measured temperatures. The temperature increase estimated with the dielectric property taken from the previous study was lower than that obtained from the measured property. Table 2 shows the calculated energy absorbance associated with the measured dielectric properties and those taken from the previous study. Our results showed that the tumor in our mouse model absorbed relatively high levels of energy (120.2 W/kg) using the measured dielectric property as compared with the energy absorbance attained using the dielectric property taken from the previous study (115.9 W/kg). Fig. 5(a,b) shows that the temperature increase in the tumor based on the calculated absorbed energy from the measured dielectric property was ~42.2 °C, whereas the temperature increase was up to 41 °C using the dielectric property taken from the previous study. In surrounding tissues, only a slight variation was observed in energy absorption and temperature distribution using the measured and dielectric properties from the previous study [Table 2 and Fig. 5(a, b)], indicating that variations in the dielectric property might not greatly affect the energy and temperature distribution. This represents an important factor in the selective heating of tumors in hyperthermia-treatment planning.

The major focus of this study was to show the effect of tumor properties on hyperthermia-treatment planning. Previous studies reported that tumors exhibit relatively high dielectric properties as compared with the normal tissues; however, some tumors show low values, which are mainly due to their high fat content (Peyman et al., 2015; Yoo, 2004). Pathological changes and different tumor stage in the same cancer subtype can result in variable dielectric properties (Li

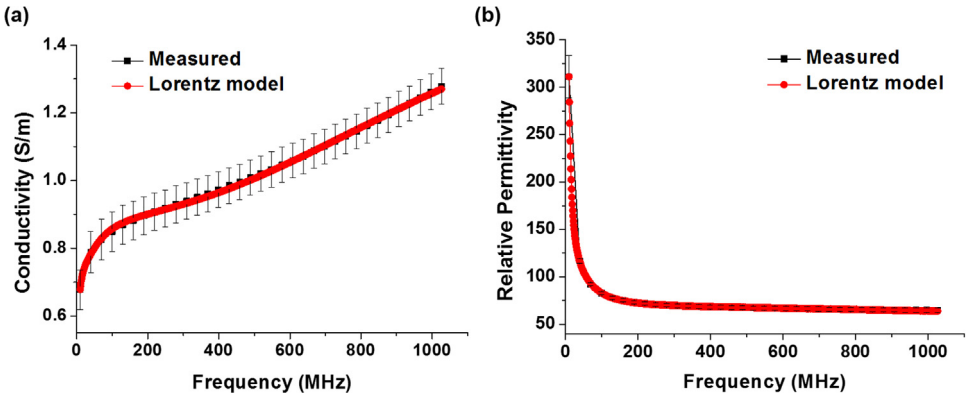

Fig. 2. (a, b) Measured and Lorentz-fitted electrical conductivity and relative permittivity of tumor tissue.

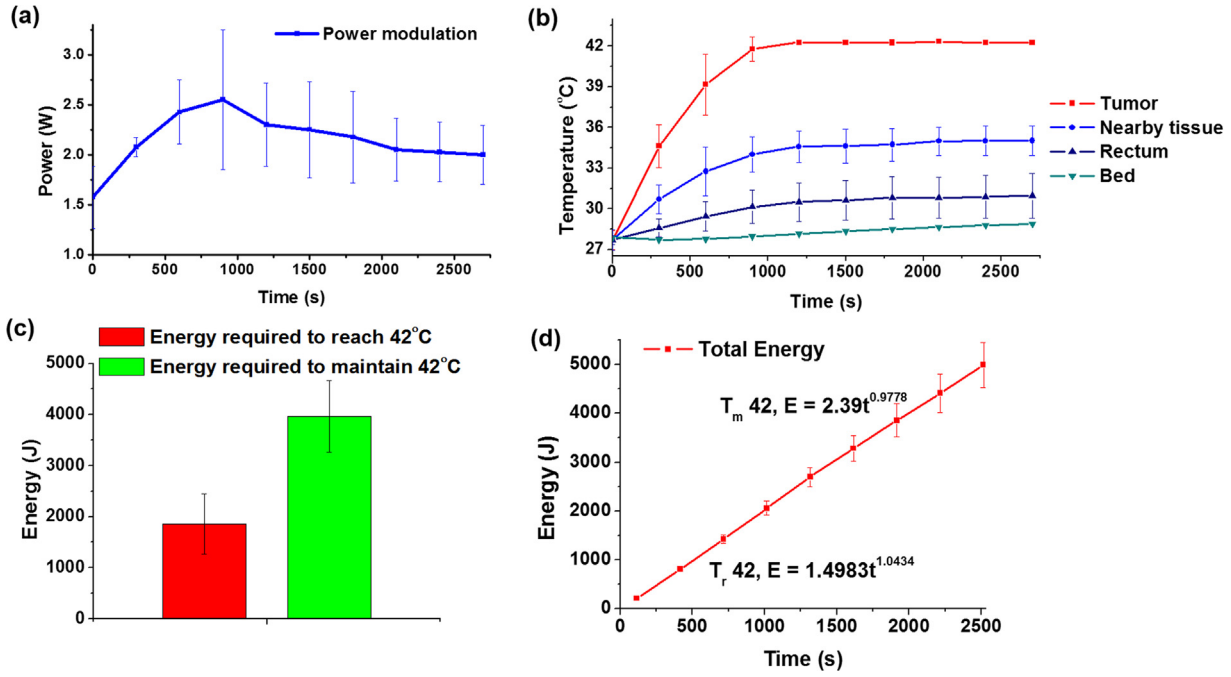

Fig. 3. (a) Output power required to reach 42 °C. (b) Temperature increase in tumor and surrounding tissues. (c) Energy estimation to achieve a temperature of 42 °C. (d) Energy/Time/Temperature relationship necessary to achieve a temperature of 42 °C.

et al., 2017; Peyman et al., 2015), and these changes need to be considered during treatment planning. Because RF hyperthermia is based on tissue-specific dielectric properties, variations in these properties affect temperature estimation and thermal-dose calculations. Temperature mapping, an effective technique that takes these effects into consideration (Kim et al., 2017), was used in experiments and simulations in our study. Since, in previous studies, dielectric properties of tumor at 13.56 MHz were reported relatively less than other frequencies and based on the difficulties in considering pathological changes and tumor stage, we used mouse-tumor properties available at 13.56 MHz from a previous study (Raoof et al., 2013) for comparative purposes. Sensitivity analysis of the effect of conductivity and permittivity is described in Supplementary Appendix 1, with the results indicating that conductivity was the dominant property associated with high energy absorption. To determine the effect of thermal properties, metabolic heat generation and perfusion analysis were performed using a modified bioheat-transfer model based on a linear temperature-dependent approximation. To determine this effect, dielectric properties were kept constant and considered the same as those of the measured properties. The coefficient of temperature-dependent enhancement of the thermal properties was considered based on the variations reported previously (Bhattacharya and Mahajan, 2003; Choi et al., 2013; Guntur et al., 2013) and with the details of the coefficients considered outlined in Supplementary Appendix 2. Variations in perfusion and metabolic heat generation were assumed to be proportional according to conventions suggested previously (Bernardi et al., 2003; Burfeindt et al., 2011; Gordon et al., 1976). However, few studies have addressed these effects on calculating thermal dose, variations of which can be much higher relative to the temperature change. Fig. 6(a,b) shows the effect of normothermal thermal properties, heat generation, and perfusion on tumor temperature (42.2 °C) as compared with temperature-dependent thermal properties, heat generation, and perfusion. The results showed that temperature variation occurred within a narrow range with an average temperature difference of 0.2 °C with normothermic property and 0.06 °C with temperature dependent properties in the mild hyperthermia-temperature range, which agreed with previous results (Guntur and Choi, 2015; Pirtini Çetingül and Herman, 2010); however, thermal-dose calculations showed significant variation. The local thermal dose calculated from normothermal properties was 233.9 min, whereas that from temperature-dependent properties was 192.3 min. The difference can be explained by the transition temperature of 43 °C used in the thermal-dose model, given that the R value will be high for temperature distributions > 43 °C (Sapareto and Dewey, 1984; van Rhoon et al., 2013). Therefore, for accurate thermal-dose calculation in treatment planning, consideration of temperature-dependent thermal properties can provide much more realistic values. Moreover, mapping of temperature distribution was also slightly improved in tumors when temperature dependence on all parameters was considered [Fig. 6(b)]. A detailed sensitivity analysis of the dependencies of individual and combined parameters is provided in Supplementary Appendix 2. The variation ranges associated with perfusion and metabolic heat generation were considered based on assumptions from previous mouse studies that perfusion will not greatly increase after reaching 41 °C due to degradation (Corr et al., 2015) and the collapse of blood vessels (Rossmann and Haemmerich, 2014). In the case of humans, increments in perfusion are reportedly higher (Waterman et al., 1991, 1987), and heat generation might also vary greatly; therefore, a coefficient based on measurements would be more realistic. Additionally, for hyperthermia therapy in the ablative temperature range, temperature dependence will be much stronger; therefore, the proposed bioheat-transfer model might not be optimal, and a more realistic model might be needed for such applications. A previous study of high-intensity focused-ultrasound ablation showed that thermal properties strongly influence the temperature distribution (Guntur et al., 2013).

Based on these approximations, an accurate thermal-dose distribution was predicted, and a comparison was made between energy absorbed from dielectric properties of tumors measured and taken from a previous study. Fig. 7(a) shows the distribution of thermal doses in mouse tumors on the XY and YZ planes. A quantitative estimation of the maximum local thermal dose is provided in Fig. 7(b). Compared with 80.14 min using the temperature obtained from the dielectric property taken from the previous study, this result showed a CEM of 192.3 min using the temperature obtained from the measured dielectric property. The thermal dose obtained from the dielectric property measured here was within a range reported in a mouse study on mammary mouse tumors in the flank and fibrosarcoma (Field and Morris, 1983; Perez

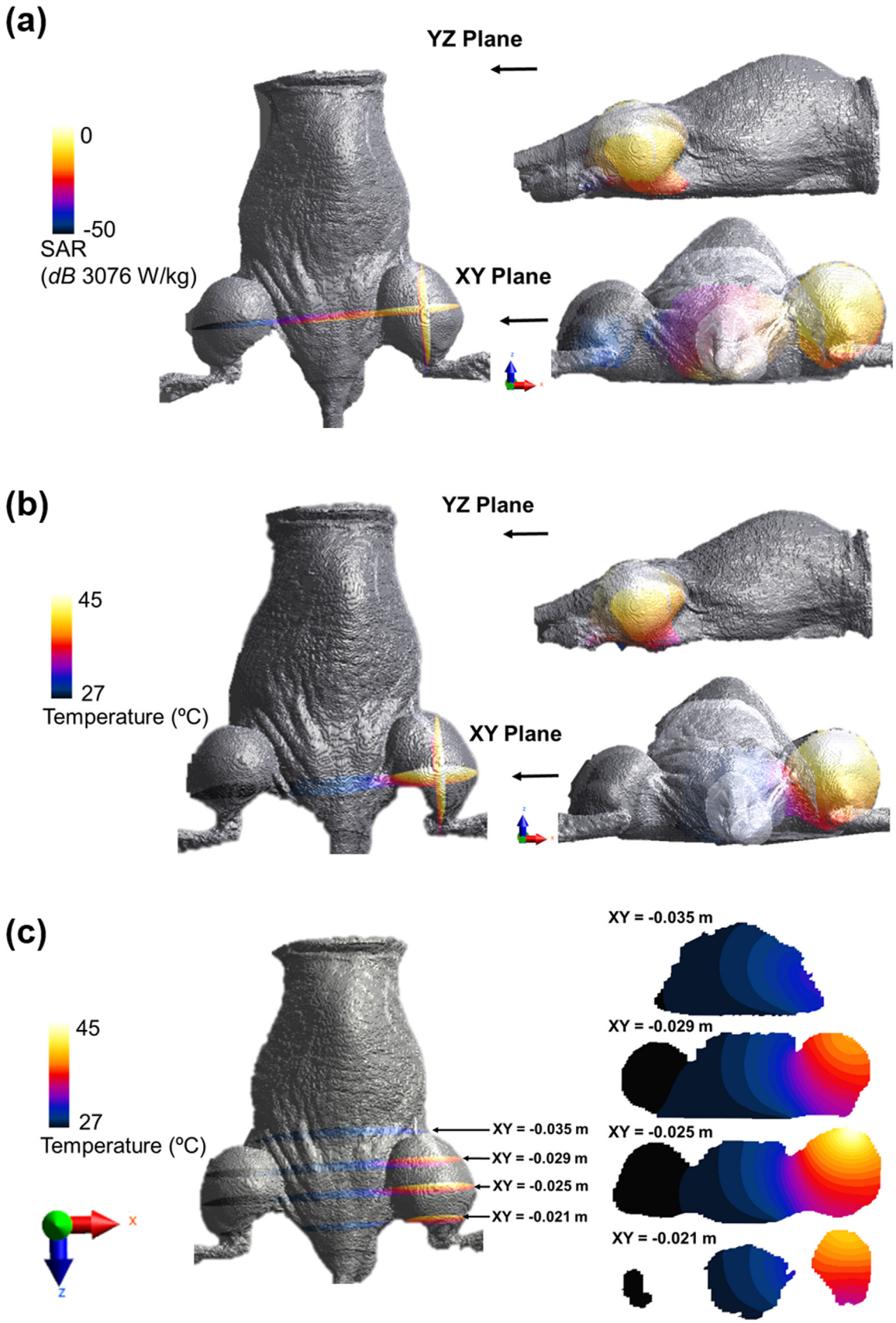

Fig. 4. (a) SAR distribution. (b) Temperature distribution along the cross-section of the mouse model. (c) Temperature distribution at different cross-sections.

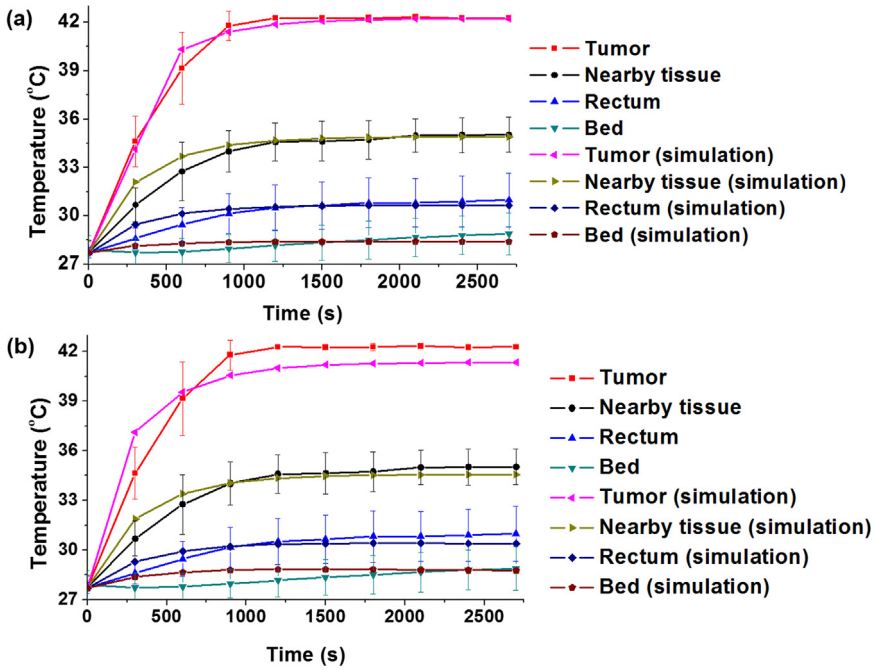

Fig. 5. Temperature mapping for the experiment and simulation. (a) Mapping using measured dielectric properties. (b) Mapping using dielectric properties taken from previous study.

Table 2
Comparison of absorbed energy with dielectric property measured and taken from previous study.

Body site	Mass-averaged SAR (W/kg)	
	Measured property	Property from previous study
Skin	7.18	6.56
Bone	0.003	0.002
Rectum	3.06	2.77
Tumor	120.27	115.91

et al., 1984), indicating that the thermal dose obtained from the measured dielectric property might be more optimal than that approximated based on the dielectric property taken from the previous study. Variations in the thermal dose based on different combinations of dielectric properties are discussed in Supplementary Appendix 1.

Temperature optimization is also very important in combined radiation and hyperthermia therapy (Kok et al., 2014; van Leeuwen et al., 2017). A previous study showed that hyperthermia is a potent radiosensitizer capable of changing the radiosensitivity parameters of cancer cell lines (Franken et al., 2013). Escalations in radiation dose are based on the targeted temperature achieved in the tumor, with underestimation or overestimation of the temperature potentially leading to inaccurate equivalent radiation-dose calculations. For example, biological modeling of thermoradiotherapy for cervical cancer in three patients using radiation doses of 45.2 Gy, 45.5 Gy, and 45.0 Gy with corresponding hyperthermia temperatures of 39.2 °C, 39.7 °C, and 40.4 °C resulted in radiation-dose escalations to 52.5 Gy, 55.5 Gy, and 56.9 Gy, respectively (Crezee et al., 2016). This result showed that temperature plays major role in equivalent radiation-dose calculations, and that it requires precise optimization for thermoradiotherapy treatment planning using accurate dielectric properties.

Obtaining patient-specific properties in clinics remains a major issue in hyperthermia-treatment planning; therefore, additional studies are needed to address this. Possible approaches include the development of an inverse method for temperature optimization based on surface-temperature measurement, optimization of tumor-tissue temperature from surrounding tissue temperature distributions, and creation of a noninvasive property measurement technique or establishment of a database of frequency specific and temperature-dependent properties associated with different tumor types and stages.

This study did not focus on therapeutic outcomes associated with hyperthermia treatment, but rather on temperature measurement and enhancing simulations based on tumor-property values. Studies on the

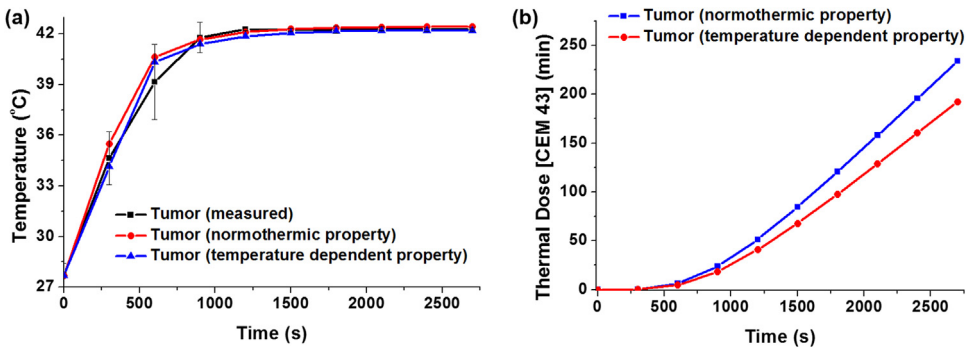

Fig. 6. (a) Comparison of temperature increases using experimental data, normothermic and temperature-dependent thermal properties, perfusion, and heat generation. (b) Comparison of thermal-dose calculations using normothermic and temperature-dependent thermal properties, perfusion, and heat generation.

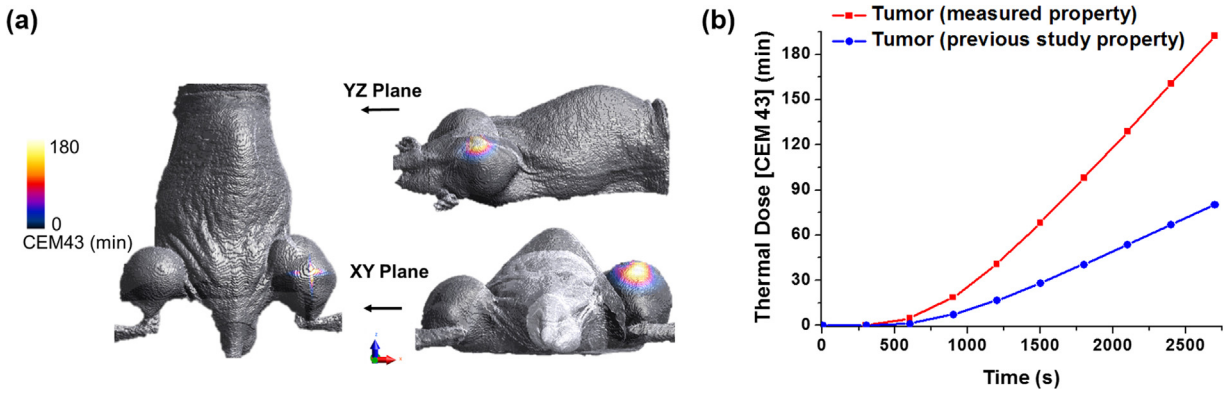

Fig. 7. (a) Thermal-dose distribution along the cross-section of the mouse model. (b) Maximum local thermal dose in tumors using measured dielectric properties and dielectric properties taken from previous study.

therapeutic outcomes associated with hyperthermia treatment and also outcomes combined with radiation therapy are currently underway in our laboratory.

4. Conclusion

The effect of tumor properties related to energy absorption, temperature mapping, and thermal dose was demonstrated numerically using a mouse xenograft model. In vivo experiments established a heating protocol allowing direct comparison with simulations, with dielectric properties measured and fitted using the Lorentz model to obtain accurate property values for simulations. We observed minimal differences in the temperature dependence of thermal properties, perfusion, and metabolic heat generation related to the modified bioheat-transfer model according to temperature distribution, although slight improvements in temperature mapping resulted in a much more precise calculation of thermal dose. Comparisons made between dielectric properties measured and those taken from previous studies showed that dielectric property variation can either underestimate or overestimate energy absorption, temperature distribution, and thermal-dose calculations; therefore, variations in dielectric property values should be considered a high priority in hyperthermia-treatment planning. These findings contribute to the development of effective thermoradiotherapy treatment-planning strategies in clinical settings.

Acknowledgements

This research was supported by the National Research Foundation sponsored by the Ministry of Science, ICT and Future Planning (NRF-2016R1A2B4012095) and the Ministry of Education (NRF-2016R1D1A1A09917195), Republic of Korea. We thank ZMT for providing a free license of Sim4Life used in this study. Bibin Prasad was funded by the Global Scholarship Program for Foreign Graduate Students at Kookmin University in Seoul, Republic of Korea.

Conflict of interest

Authors have no conflict of interest.

Appendix A. Supporting information

Supplementary data associated with this article can be found in the online version at http://dx.doi.org/10.1016/j.jtherbio.2018.04.007.

References

Ahmed, M., Liu, Z., Humphries, S., Goldberg, S.N., 2008. Computer modeling of the combined effects of perfusion, electrical conductivity, and thermal conductivity on tissue heating patterns in radiofrequency tumor ablation. Int. J. Hyperth. 24, 577–588. http://dx.doi.org/10.1080/02656730802192661.

Banks, H., Bokil, V., Gibson, N., 2008. Analysis of stability and dispersion in a finite element method for Debye and Lorentz dispersive media. Numer. methods partial differ. Numer. Methods Partial Differ. Equation 25, 885–917. http://dx.doi.org/10.1002/num.

Bernardi, P., Cavagnaro, M., Pisa, S., Piuzzi, E., 2003. Specific absorption rate and temperature elevation in a subject exposed in the far-field of radio-frequency sources operating in the 10–900-MHz range. IEEE Trans. Biomed. Eng. 50, 295–304. http://dx.doi.org/10.1109/TBME.2003.808809.

Bhattacharya, a., Mahajan, R., 2003. Temperature dependence of thermal conductivity of biological tissues. Physiol. Meas. 24, 769–783. http://dx.doi.org/10.1088/0256-307X/25/9/060.

Burfeindt, M.J., Zastrow, E., Hagness, S.C., Van Veen, B.D., Medow, J.E., 2011. Microwave beamforming for non-invasive patient-specific hyperthermia treatment of pediatric brain cancer. Phys. Med. Biol. 56, 2743–2754. http://dx.doi.org/10.1088/0031-9155/56/9/007.

Choi, J., Morrissey, M., Bischof, J.C., 2013. Thermal processing of biological tissue at high temperatures: impact of protein denaturation and water loss on the thermal properties of human and porcine liver in the range 25–80 °C. J. Heat Transf. 135, 61302. http://dx.doi.org/10.1115/1.4023570.

Corr, S.J., Shamsudeen, S., Vergara, L.A., Chak-Shing Ho, J., Ware, M.J., Keshishian, V., Yokoi, K., Savage, D.J., Meraz, I.M., Kaluarachchi, W., Cisneros, B.T., Raoof, M., Nguyen, D.T., Zhang, Y., Wilson, L.J., Summers, H., Rees, P., Curley, S.A., Serda, R.E., 2015. A new imaging platform for visualizing biological effects of non-invasive radiofrequency electric-field cancer hyperthermia. PLoS One 10, 1–16. http://dx.doi.org/10.1371/journal.pone.0136382.

Crezee, J., van Leeuwen, C.M., Oei, A.L., van Heerden, L.E., Bel, A., Stalpers, L.J.A., Ghadjar, P., Franken, N.A.P., Kok, H.P., 2016. Biological modelling of the radiation dose escalation effect of regional hyperthermia in cervical cancer. Radiat. Oncol. 11, 14. http://dx.doi.org/10.1186/s13014-016-0592-z.

Field, S.B., Morris, C.C., 1983. The relationship between heating time and temperature: its relevance to clinical hyperthermia. Radiother. Oncol. 1, 179–186. http://dx.doi.org/10.1016/S0167-8140(83)80020-6.

Foster, K.R., Schepps, J.L., 1981. Dielectric properties of tumor and normal tissues at radio through microwave frequencies. J. Microw. Power1 16, 107–119. http://dx.doi.org/10.1080/16070658.1981.11689230.

Franken, N.A.P., Oei, A.L., Kok, H.P., Rodermond, H.M., Sminia, P., Crezee, J., Stalpers, L.J.A., Barendsen, G.W., 2013. Cell survival and radiosensitisation: modulation of the linear and quadratic parameters of the LQ model (Review). Int. J. Oncol. 42, 1501–1515. http://dx.doi.org/10.3892/ijo.2013.1857.

Gabriel, S., Lau, R.W., Gabriel, C., 1996a. The dielectric properties of biological tissues: II. measurements in the frequency range 10 Hz to 20 GHz. Phys. Med. Biol. 41, 2251–2269. http://dx.doi.org/10.1088/0031-9155/41/11/002.

Gabriel, S., Lau, R.W., Gabriel, C., 1996b. The dielectric properties of biological tissues: III. Parametric models for the dielectric spectrum of tissues. Phys. Med. Biol. 41, 2271–2293. http://dx.doi.org/10.1088/0031-9155/41/11/003.

Gabriel, C., Gabriel, S., Corthout, E., 1996c. The dielectric properties of biological tissues: I. Literature survey. Phys. Med. Biol. 41, 2231–2249.

Gordon, R.G., Roemer, R.B., Horvath, S.M., 1976. A mathematical model of the human temperature regulatory system–transient cold exposure response. IEEE Trans. Biomed. Eng. 23, 434–444. http://dx.doi.org/10.1109/TBME.1976.324601.

Guntur, S.R., Choi, M.J., 2015. Influence of temperature-dependent thermal parameters on temperature elevation of tissue exposed to high-intensity focused ultrasound: numerical simulation. Ultrasound Med. Biol. 41, 806–813. http://dx.doi.org/10.1016/j.ultrasmedbio.2014.10.008.

Guntur, S.R., Lee, K., Il, Paeng, D.-G., Coleman, A.J., Choi, M.J., 2013. Temperature-dependent thermal properties of ex vivo liver undergoing thermal ablation. Ultrasound Med. Biol. 39, 1771–1784. http://dx.doi.org/10.1016/j.ultrasmedbio.2013.04.014.

Hasgall P.A., Di Gennaro F., Baumgartner C., Neufeld E., Gosselin M.C., Payne D., Klingenböck A., Kuster, N., 2015. IT'IS Database for Thermal and Electromagnetic Parameters of Biological Tissues [WWW Document]. https://doi.org/10.13099/VIP21000-03-0.

Hossain, M.T., Prasad, B., Park, K.S., Lee, H.J., Ha, Y.H., Lee, S.K., Kim, J.K., 2016. Simulation and experimental evaluation of selective heating characteristics of 13.56 MHz radiofrequency hyperthermia in phantom models. Int. J. Precis. Eng. Manuf. 17, 253–256. http://dx.doi.org/10.1007/s12541-016-0033-9.

Joines, W.T., Zhang, Y., Li, C., Jirtle, R., 1994. The measured electrical properties of normal and malignant human tissues from 50 to 900 MHz. Med. Phys. 24, 547–550.

Kim, K.S., Lee, S.Y., 2015. Nanoparticle-mediated radiofrequency capacitive hyperthermia: a phantom study with magnetic resonance thermometry. Int. J. Hyperth. 31, 831–839. http://dx.doi.org/10.3109/02656736.2015.1096968.

Kim J.K., Prasad B., Kim S., Temperature mapping and thermal dose calculation in combined radiation therapy and 13.56 MHz radiofrequency hyperthermia for tumor treatment, Proc. SPIE 10047,1004718, 2017, https://doi.org/10.1117/12.2253163.

Kim, W., Kim, M.-S., Kim, H., Lee, E., Jeong, J., Park, I., Jeong, Y.K., Jang, W.I., 2018. Role of HIF-1α in response of tumors to a combination of hyperthermia and radiation *in vivo*. Int. J. Hyperth. 34, 276–283. http://dx.doi.org/10.1080/02656736.2017.1335440.

Kok, H.P., Crezee, J., 2017. A comparison of the heating characteristics of capacitive and radiative superficial hyperthermia. Int. J. Hyperth. 33, 378–386. http://dx.doi.org/10.1080/02656736.2016.1268726.

Kok, H.P., Crezee, J., Franken, N.A.P., Stalpers, L.J.A., Barendsen, G.W., Bel, A., 2014. Quantifying the combined effect of radiation therapy and hyperthermia in terms of equivalent dose distributions. Int. J. Radiat. Oncol. Biol. Phys. 88, 739–745. http://dx.doi.org/10.1016/j.ijrobp.2013.11.212.

Kok, H.P., Kotte, A.N.T.J., Crezee, J., 2017. Planning, optimisation and evaluation of hyperthermia treatments. Int. J. Hyperth. 33, 593–607. http://dx.doi.org/10.1080/02656736.2017.1295323.

Li, Z., Wang, W., Cai, Z., Han, S., Lin, S., He, L., Chen, M., Pan, D., Deng, G., Duan, S., Xin, S.X., 2017. Variation in the dielectric properties of freshly excised colorectal cancerous tissues at different tumor stages. Bioelectromagnetics 38, 522–532. http://dx.doi.org/10.1002/bem.22066.

Oh, S., Ryu, Y.C., Carluccio, G., Sica, C.T., Collins, C.M., 2014. Measurement of SAR-induced temperature increase in a phantom and in vivo with comparison to numerical simulation. Magn. Reson. Med. 71, 1923–1931. http://dx.doi.org/10.1002/mrm.24820.

Paulides, M.M., Stauffer, P.R., Neufeld, E., Maccarini, P.F., Kyriakou, A., Canters, R. a.M., Diederich, C.J., Bakker, J.F., Van Rhoon, G.C.,, 2013. Simulation techniques in hyperthermia treatment planning. Int. J. Hyperth. 29, 346–357. http://dx.doi.org/10.3109/02656736.2013.790092.

Pennes, H., 1948. Analysis of tissue and arterial blood temperatures in the resting human forearm. J. Appl. Physiol. 1, 93–122.

Perez, C.A., Sapareto, S.A., Control, T.R., 1984. Thermal Dose Expression in Clinical Hyperthermia and Correlation with Tumor Response/Control. Cancer Res. 44, 4818–4826.

Peyman, A., Kos, B., Djokić, M., Trotovšek, B., Limbaeck-Stokin, C., Serša, G., Miklavčič, D., 2015. Variation in dielectric properties due to pathological changes in human liver. Bioelectromagnetics 36, 603–612. http://dx.doi.org/10.1002/bem.21939.

Pirtini Çetingül, M., Herman, C., 2010. A heat transfer model of skin tissue for the detection of lesions: sensitivity analysis. Phys. Med. Biol. 55, 5933–5951. http://dx.doi.org/10.1088/0031-9155/55/19/020.

Prasad, B., Ha, Y.H., Lee, S.K., Kim, J.K., 2016. Patient-specific simulation for selective liver tumor treatment with noninvasive radiofrequency hyperthermia. J. Mech. Sci. Technol. 30, 5837–5845. http://dx.doi.org/10.1007/s12206-016-1154-x.

Rai, K.N., Rai, S.K., 1999. Effect of metabolic heat generation and blood perfusion on the heat transfer in the tissues with a blood vessel. Heat Mass Transf. 35, 75–79. http://dx.doi.org/10.1007/s002310050300.

Raoof, M., Cisneros, B.T., Corr, S.J., Palalon, F., Curley, S.A., Koshkina, N.V., 2013. Tumor selective hyperthermia induced by short-wave capacitively-coupled RF electric-fields. PLoS One 8, 1–9. http://dx.doi.org/10.1371/journal.pone.0068506.

Rogers, J.A., Sheppard, R.J., Grant, E.H., Bleehen, N.M., Honess, D.J., 1983. The dielectric properties of normal and tumour mouse tissue between 50 MHz and 10 GHz. Br. J. Radiol. 56, 335–338. http://dx.doi.org/10.1259/0007-1285-56-665-335.

Rossmann, C., Haemmerich, D., 2014. Review of temperature dependence of thermal properties, dielectric properties, and perfusion of biological tissues at hyperthermic and ablation temperatures. Crit. Rev. Biomed. Eng. 42, 467–492. http://dx.doi.org/10.1002/jmri.23741.Proton.

Sapareto, S.A., Dewey, W.C., 1984. Thermal dose determination in cancer therapy. Int. J. Radiat. Oncol. Biol. Phys. 10, 787–800. http://dx.doi.org/10.1016/0360-3016(84)90379-1.

Stoykov, N.S., Kuiken, T.A., Lowery, M.M., Taflove, A., 2003. Finite-element time-domain algorithms for modeling linear Debye and Lorentz dielectric dispersions at low frequencies. IEEE Trans. Biomed. Eng. 50, 1100–1107. http://dx.doi.org/10.1109/TBME.2003.816083.

Sullivan, D.M., 1992. Frequency-dependent FDTD methods using Z transforms. IEEE Trans. Antennas Propag. 40, 1223–1230. http://dx.doi.org/10.1109/8.182455.

Tomura, K., Ohguri, T., Mulder, H.T., Murakami, M., Nakahara, S., Yahara, K., Korogi, Y., 2017. The usefulness of mobile insulator sheets for the optimisation of deep heating area for regional hyperthermia using a capacitively coupled heating method: phantom, simulation and clinical prospective studies. Int. J. Hyperth. 0, 1–12. http://dx.doi.org/10.1080/02656736.2017.1402130.

Tsuda, N., Kuroda, K., Suzuki, Y., 1996. An inverse method to optimize heating conditions in RF-capacitive hyperthermia. IEEE Trans. Biomed. Eng. 43, 1029–1037. http://dx.doi.org/10.1109/10.536904.

van der Zee, J., 2002. Heating the patient: a promising approach? Ann. Oncol. 13, 1173–1184. http://dx.doi.org/10.1093/annonc/mdf280.

van Leeuwen, C.M., Crezee, J., Oei, A.L., Franken, N.A.P., Stalpers, L.J.A., Bel, A., Kok, H.P., 2017. 3D radiobiological evaluation of combined radiotherapy and hyperthermia treatments. Int. J. Hyperth. 33, 160–169. http://dx.doi.org/10.1080/02656736.2016.1241431.

van Rhoon, G.C., Samaras, T., Yarmolenko, P.S., Dewhirst, M.W., Neufeld, E., Kuster, N., 2013. CEM 43 °C thermal dose thresholds: a potential guide for magnetic resonance radiofrequency exposure levels? Eur. Radiol. 23, 2215–2227. http://dx.doi.org/10.1007/s00330-013-2825-y.

Waterman, F.M., Nerlinger, R.E., Moylan, D.J., 3Rd, Leeper, D.B., 1987. Response of human tumor blood flow to local hyperthermia. Int. J. Radiat. Oncol. Biol. Phys. 13, 75–82.

Waterman, F.M., Tupchong, L., Phil, D., Nerlinger, R.E., Matthews, J., 1991. Blood flow in human tumors during local hyperthermia. Int. J. Radiat. Oncol. Biol. Phys. 20, 1255–1262.

Yoo, D.S., 2004. The dielectric properties of cancerous tissues in a nude mouse xenograft model. Bioelectromagnetics 25, 492–497. http://dx.doi.org/10.1002/bem.20021.

Zastrow, E., Hagness, S.C., Van Veen, B.D., 2010. 3D computational study of non-invasive patient-specific microwave hyperthermia treatment of breast cancer. Phys. Med. Biol. 55, 3611–3629. http://dx.doi.org/10.1088/0031-9155/55/13/003.

Zorbas, G., Samaras, T., 2014. Simulation of radiofrequency ablation in real human anatomy. Int. J. Hyperth. 30, 570–578. http://dx.doi.org/10.3109/02656736.2014.968639.